Articles

Outer Sphere Mutations Perturb Metal Reactivity in Manganese Superoxide Dismutase[†,‡]

Ross A. Edwards,[§] Mei M. Whittaker,[||] James W. Whittaker,*[,||] Edward N. Baker,*[,⊥] and Geoffrey B. Jameson*[,§]

Centre for Structural Biology, Institutes of Fundamental Sciences and Molecular BioSciences, Massey University, Palmerston North, New Zealand, Department of Biochemistry and Molecular Biology, Oregon Graduate Institute of Science & Technology, 20000 Northwest Walker Road, Beaverton, Oregon 97006-8921, and School of Biological Sciences and Department of Chemistry, University of Auckland, Auckland, New Zealand

Received August 14, 2000

ABSTRACT: Tyrosine 34 and glutamine 146 are highly conserved outer sphere residues in the mononuclear manganese active site of *Escherichia coli* manganese superoxide dismutase. Biochemical and spectroscopic characterization of site-directed mutants has allowed functional characterization of these residues in the wild-type (wt) enzyme. X-ray crystallographic analysis of three mutants (Y34F, Q146L, and Q146H) reveal subtle changes in the protein structures. The Y34A mutant, as well as the previously reported Y34F mutant, retained essentially the full superoxide dismutase activity of the wild-type enzyme, and the X-ray crystal structure of Y34F manganese superoxide dismutase shows that mutation of this strictly conserved residue has only minor effects on the positions of active site residues and the organized water in the substrate access funnel. Mutation of the outer sphere solvent pocket residue Q146 has more dramatic effects. The Q146E mutant is isolated as an apoprotein lacking dismutase activity. Q146L and Q146H mutants retain only 5−10% of the dismutase activity of the wild-type enzyme. The absorption and circular dichroism spectra of the Q146H mutant resemble corresponding data for the superoxide dismutase from a hyperthermophilic archaeon, *Pyrobaculum aerophilum*, which is active in both Mn and Fe forms. Interestingly, the iron-substituted Q146H protein also exhibits low dismutase activity, which increases at lower pH. Mutation of glutamine 146 disrupts the hydrogen-bonding network in the active site and has a greater effect on protein structure than does the Y34F mutant, with rearrangement of the tyrosine 34 and tryptophan 128 side chains.

Superoxide dismutases (SODs)[1] are ubiquitous antioxidant metalloenzymes that catalyze disproportionation of superoxide through a one-electron redox cycle (*1*−*3*).

$$2O_2^{-\bullet} + 2H^+ \rightarrow O_2 + H_2O_2$$

This radical-scavenging function protects biological systems from oxidative damage produced by toxic oxygen metabolites. Four different kinds of redox active metal cofactors have been found in superoxide dismutases: Cu−Zn, Fe, Mn, and Ni (*4*−*7*). FeSOD and MnSOD share both amino acid sequence and three-dimensional structural homology (*8*−*10*), while the other superoxide dismutases are structurally unrelated. Despite the high degree of structural homology between Fe- and MnSODs, these enzymes generally require a specific metal ion (either Mn or Fe) for activity (*9*) and the structural basis for this specificity remains elusive (*11*, *12*). A small number of *cambialistic* enzymes, which are active with either Fe or Mn, are exceptions to this strict metal ion specificity (*13*−*20*).

High-resolution crystal structures have been determined for four MnSODs [from *Thermus thermophilus* (1.8 Å) (*21*, *22*), *Bacillus stearothermophilus* (2.4 Å) (*23*), human mitochondria (2.2 Å) (*24*, *25*), and *Escherichia coli* (2.0 Å) (*26*)], four FeSODs [from *E. coli* (1.8 Å) (*27*−*29*), *Pseudomonas ovalis* (2.1 Å) (*30*−*32*), *Mycobacterium tuberculosis* (2.0 Å) (*33*), and the hyperthermophilic bacterium *Aquifex pyrophilus* (1.9 Å) (*34*)], and two cambialistic SODs [from *Propionibacterium shermanii* (1.6 Å) (*35*) and *Porphyromonas gingivalis* (1.8 Å) (*36*)]. Recently, crystal structures

[†] This work is supported by grants from the Marsden Fund of New Zealand (Grant MAU606 to G.B.J. and E.N.B.), the Lottery Health Grants Board of New Zealand (to G.B.J.), and the National Institutes of Health (Grant GM42680 to J.W.W.).

[‡] Atomic coordinates have been deposited with the Protein Data Bank, with accession codes 1en5 (Y34F), 1en4 (Q146H), and 1en6 (Q146L).

* To whom correspondence should be addressed. G.B.J.: telephone, (+64) 6 350-4431; fax, (+64) 6 350-5682; e-mail, G.B.Jameson@massey.ac.nz. E.N.B.: telephone, (+64) 9 373-7599; fax, (+64) 9 373-7619; e-mail, Ted.Baker@auckland.ac.nz. J.W.W.: telephone, (503) 690-1065; fax, (503) 690-1464; e-mail, jim@bmb.ogi.edu.

[§] Massey University.

[||] Oregon Graduate Institute of Science & Technology.

[⊥] University of Auckland.

[1] Abbreviations: CD, circular dichroism; EPR, electron paramagnetic resonance; LMCT, ligand-to-metal charge transfer; MCD, magnetic circular dichroism; NIR, near-infrared; rms, root-mean-square; SOD, superoxide dismutase; UV, ultraviolet; wt, wild-type.

10.1021/bi0018943 CCC: $20.00
Published on Web 12/07/2000

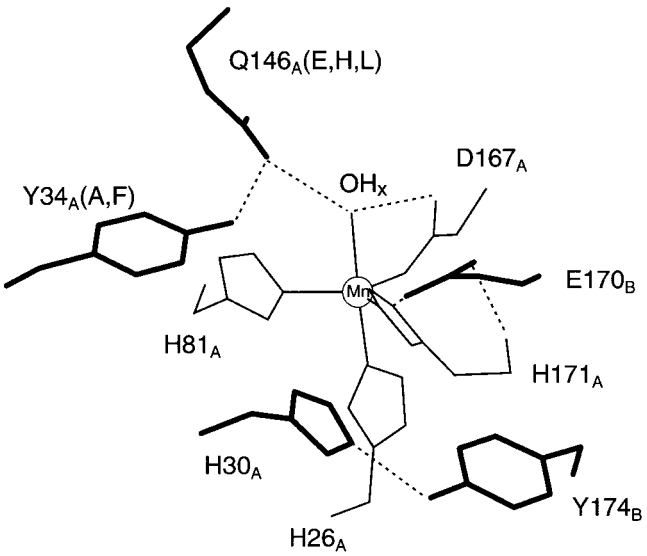

FIGURE 1: Active site structure of *E. coli* MnSOD. Second-shell residues are highlighted in bold.

have been determined for two hyperthermophilic archael FeSODs [from *Sulfolobus solfataricus* (2.3 Å) (*37*) and *Sulfolobus acidocaldarius* (2.2 Å) (*38*)]. The active site structures of Fe- and MnSODs are highly conserved, and nearly identical. Mn and Fe are coordinated in their respective enzymes by three histidines (His26, His81, and His171) and an aspartic acid, Asp167 [numbering throughout this paper refers to the *E. coli* MnSOD numbering scheme (*26*, *39*)]. A solvent molecule (water or hydroxide) is also coordinated to the metal (*26*), and is fixed in place by two hydrogen bonds. The solvent is the donor of a hydrogen bond with the noncoordinated oxygen of Asp167 OD1 and serves as the acceptor of a hydrogen bond from Gln146 NE2. Additional hydrogen bonds are formed between Gln146 NE2 and the hydroxyl group of Tyr34, and between Gln146 OE1 and Asn80 ND2 and Trp128 NE1. Gln146 is, therefore, a key component of an extended hydrogen-bonding network around the active site (Figure 1).

Recently, site-directed mutagenesis has been used to investigate the functional role of individual protein residues in Fe- and MnSOD through site-specific amino acid substitutions (*40*−*51*).[2]

For the Y34F (*45*), W161F (*47*), Q143N (*46*), Q143A (*49*), and H30N (*48*) mutants of the MnSOD from human mitochondria, high-resolution X-ray structures (1.9, 2.3, 2.3, 2.13, and 2.3 Å, respectively) have been determined. Rather lower-resolution structures (2.5 and 4.0 Å) are available for the H145E and H145Q mutants of the FeSOD from *M. tuberculosis* (*50*).

In general, mutation of residues in the second coordination sphere of the active site metal center may have a significant effect on the catalytic activity but relatively little effect on the conformation of the enzyme or on active site structure. Mutation of the bridging outer sphere counterion Glu170 to alanine in *E. coli* MnSOD is an exception that destabilizes the dimer structure and affects metal binding selectivity (*43*). Here we combine structural, spectroscopic, and biochemical methods to characterize a series of *E. coli* MnSOD mutants. In this paper, we present results on mutants involved in the putative proton relay, including the coordinated OH^-/H_2O, Gln146, Tyr34, and solvent: specifically, Y34A, Q146E, Q146H, and Q146L. X-ray structures at 2.0 Å resolution have been determined for Q146H and Q146L mutants, as well as for Y34F (to 2.3 Å resolution), whose biochemical and spectroscopic characterization has previously been reported (*42*, *52*). In the Y34F mutant of *E. coli* MnSOD and human mitochondrial MnSOD, hydrogen bonding of the hydroxyl group to Gln146 is eliminated. The effects of replacing Gln146 with histidine, which is the side chain found in several Mn- and FeSODs, are investigated in the Q146H mutant of *E. coli* MnSOD, a system complementary to the H146Q mutant of *M. tuberculosis* FeSOD (*50*). The complete elimination of the putative proton relay between Tyr34 and the coordinated OH^-/H_2O moiety is investigated with the approximately isosteric Q146L mutant. Our results on these *E. coli* MnSOD mutants are combined with results on other species to give new and unexpected insights into the roles that Tyr34 and Gln146 play in active site chemistry.

MATERIALS AND METHODS

Biochemical Preparation. The pDT1-5 plasmid containing the *sodA* locus (*53*) was a generous gift from D. Touati (Institut Jacques Monod, Centre National de la Recherche Scientifique, Universite Paris VII, Paris, France). This plasmid was used as a template for the production of all mutant plasmids using the Stratagene QuickChange *in vitro* site-directed mutagenesis procedure as previously described (*27*). Sequences of the mutant plasmids were verified by DNA sequence analysis (Molecular Biology Core Facility, Oregon Primate Research Center, Beaverton, OR) of the entire structural gene. The mutant plasmids were transformed into *E. coli* QC781 (*54*) sod A^- cells for protein expression. *E. coli* cells were grown as described previously (*43*), except the medium was supplemented with either 1 mM Mn(II) salts or 1 mM Fe(II) salts. Superoxide dismutase was purified as described previously (*52*). pH titration of Q146H- and Q146L-Mn(III)SOD was carried out as described previously (*42*), except Bicine/KOH buffer was not used for Q146L-MnSOD due to the susceptibility of this mutant to reduction of Mn(III) to Mn(II) by Bicine. SOD activity was measured using the xanthine oxidase/cytochrome *c* inhibition assay (*4*). Protein concentrations were determined by optical absorption measurements using the previously reported molar extinction coefficient ($A_{280} = 8.66 \times 10^4\ M^{-1}\ cm^{-1}$) (*55*). Metal quantitation was accomplished by atomic absorption spectrometric analysis using a Varian SpectrAA 20B atomic absorption spectrometer equipped with a GTA-96 graphite furnace.

Spectroscopic Measurements. Optical absorption spectra of the proteins were recorded on a Varian Cary5 UV−vis−NIR absorption spectrometer. CD and MCD spectra were recorded using an AVIV Associates model 40DS UV−vis−NIR dichrometer as previously described (*52*). An Oxford Instruments SM4-6T magnetocryostat provided the magnetic field and temperature control during MCD spectroscopy. The mutant proteins were converted to the oxidized Mn(III) form before optical spectrometry by treating the sample with excess molybdicyanide (*52*) or with 2 equiv of sodium *m*-periodate, followed with desalting by gel filtration. EPR

[2] Positions 143 of human mitochondrial MnSOD and 145 of FeSOD from *M. tuberculosis* are structurally equivalent to position 146 of MnSOD from *E. coli*.

Table 1: Data Collection and Reduction Statistics for *E. coli* Y34F-, Q146H-, and Q146L-MnSOD[a]

	Y34F-MnSOD	Q146H-MnSOD	Q146L-MnSOD
space group	$C222_1$	$C222_1$	$C222_1$
Z (Z')	32 (4)	32 (4)	32 (4)
unit cell dimensions (Å)	$a = 100.84$	$a = 100.77$	$a = 101.70$
	$b = 108.89$	$b = 109.24$	$b = 109.30$
	$c = 182.88$	$c = 180.89$	$c = 181.72$
$V(m)$ (Å^3/Da)	2.79	2.79	2.81
solvent content (%)	56	56	56
mosaicity (deg)	0.30	0.20	0.21
data collection temperature (K)	293	293	293
data processing			
resolution limits (Å) (last shell)	40−2.3 (2.33−2.30)	40−2.0 (2.05−2.00)	40−2.0 (2.05−2.00)
no. of unique reflections	45092	68276	68589
no. of observed reflections	348981	400712	812160
no. of observed reflections after averaging	242697	227560	609197
no. of observed reflections after averaging ($I > 1\sigma_I$)	241639	220099	609136
no. of observed reflections after merging	43949	65122	66399
no. of observations deleted manually[b]	116	210	3423
redundancy	5.5	3.5	9.2
completeness (%)	97.5 (79.2)	95.4 (86.0)	96.8 (87.4)
R_{merge} on intensities	0.087 (0.298)	0.051 (0.327)	0.067 (0.255)
overall I/σ	17.2 (3.2)	19.8 (4.5)	34.4 (4.7)

[a] $R_{merge} = \Sigma\Sigma|I - \langle I\rangle|/\Sigma I$, where $\langle I\rangle$ is the mean of the number of individual observations of intensities I. [b] Deleted as outliers in averaging. In addition, because exposure times were quadrupled for data collection on the second crystal of Q146L, data at resolution worse than 4.0 Å were deleted.

spectra were recorded on a Varian E-109 X-band EPR spectrometer equipped with an Air Products He cryostat. The mutant protein was converted to the Mn(II) form for EPR spectroscopy by dithionite reduction, followed by anaerobic desalting.

Crystallization. Y34F crystals were grown using the method of hanging-drop diffusion at room temperature. The well solution was 20% (w/v) PEG 6000, 0.1 M Bicine (pH 8.3), and 25 mM NaN_3. Drops were comprised of 2 μL of well solution and 2 μL of protein solution (concentration of 9.0 mg/mL in water). Crystals of Q146H and Q146L were grown at room temperature using the method of sitting-drop vapor diffusion. The reservoir solution was 0.1 M Bicine at pH 8.0 containing PEG 6000 (20% w/v). The crystallization well contained initially 40 mM Bicine at pH 8.0, 8% (w/v) PEG 6000, and protein (concentration of 11 mg/mL for Q146L and 20 mg/mL for Q146H). Crystals were typically thick needles having dimensions of approximately 0.25 mm $\times$ 0.30 mm $\times$ 1.2 mm.

X-ray Diffraction, Data Collection, and Structure Refinement. Data for all three mutants were collected on a Rigaku R-Axis IIC image plate detector, using graphite-monochromated Cu Kα radiation from a Rigaku RU-200B rotating anode generator. Data for all mutants were processed and scaled using the programs DENZO and SCALEPACK (*56*). The data were put on an approximately absolute scale using the scale factor taken from a Wilson plot. Relevant data collection and processing statistics for all mutants are given in Table 1. The crystals were all isomorphous with each other (and with wt MnSOD from *E. coli*), in space group $C222_1$ and with two dimers in the asymmetric unit. For Y34F-MnSOD, data were collected to 2.3 Å resolution from a single crystal at room temperature, for Q146L-MnSOD from two crystals at room temperature, and for Q146H-MnSOD from a single crystal at room temperature. For both Q146L and Q146H mutants, the crystals were sufficiently large to be translated during data collection when the part of the crystal exposed to X-rays had suffered significant radiation damage.

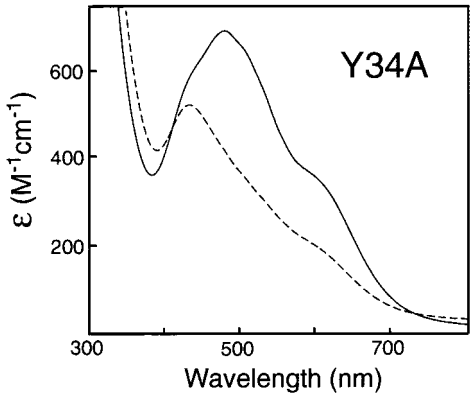

FIGURE 2: Optical absorption spectra of Y34A-Mn(III)SOD. Protein (0.5 mM active site) in 50 mM potassium phosphate buffer at pH 7.0: (—) Y34A after treatment with 2 equiv of $NaIO_4$ and (- - -) Y34A plus 100 mM NaN_3 ($K_d = 4$ mM).

As all mutants and the wt MnSOD were isomorphous, a common set of reflections was used in the calculation of R_{free}. The initial model for Y34F-MnSOD was created from wt MnSOD (*26*) by removing the metal ions, all solvent water molecules, and the side chains of all residues within a 10 Å sphere of Phe34. Final least-squares refinements of Y34F-, Q146H-, and Q146L-MnSOD were carried out with CNS (*57*), with NCS restraints on positional and thermal parameters of the four subunits. Refinement and model statistics are given in Table 2. The structure of the Q146L mutant was determined using the molecular replacement program AMORE (*58*) with the structure of wt dimeric MnSOD as the search model. The structure of Q146L-MnSOD was used as the starting model for refinement of Q146H-MnSOD; bias was removed by an initial round of automated torsion-angle simulated-annealing refinement against maximum-likelihood targets with CNS (*57*).

Table 2: Refinement and Model Statistics for *E. coli* Y34F-, Q146H-, and Q146L-MnSOD

	Y34F	Q146H	Q146L
PDB entry	1EN5	1EN4	1EN6
no. of residues	820	820	820
no. of protein atoms	6508	6516	6528
no. of water molecules	303	444	300
no. of Mn ions	4	4	4
average *B*-factors (Å^2)			
main chain atoms	24.1	25.8	29.9
side chain atoms	25.6	25.1	31.9
water molecules	27.4	34.4	35.5
Mn	11.6	13.5	16.9
overall	25.0	26.0	31.0
refinement			
program	CNS version 0.5 (*59*)	CNS version 0.4 (*59*)	CNS version 0.5 (*59*)
no. of reflections used in refinement	43928	65109	66352
no. of reflections used in calculation of R_{free}	2220 (5.1%)	3182 (4.9%)	3258 (4.9%)
resolution limits (Å)	40.0−2.3	40.0−2.0	40.0−2.0
rms for bond lengths (Å)	0.005	0.005	0.006
rms for bond angles (deg)	1.19	1.16	1.13
Ramachandran plot (*61*) (%)			
most favored region	89.8	90.4	91.9
additional allowed regions	9.1	8.2	6.6
generously allowed regions	0.6	0.8	1.1
disallowed regions	0.6	0.6	0.4
main chain rms deviations			
monomer vs monomer for mutant (Å)	0.15−0.35	0.14−0.43	0.16−0.48
dimers of mutant vs dimers of wt (Å)	0.30−0.55	0.38−0.61	0.39−0.65
R-factor (all data)	0.164	0.192	0.189
R_{free} (all data)	0.192	0.211	0.214

Table 3: Catalytic Activity for *E. coli* Mutants

	SOD activity (units/mg)	
MnSOD mutant	Mn	Fe
wt	7300	60
Y34F	6000	850
Y34A	7300	170
Q146H (pH 7.8)	600	430
Q146H (pH 6.5)	590	1050
Q146L	340	120
Q146E	−	−

RESULTS

Superoxide Dismutase Activity. With the exception of Y34A-MnSOD, the Mn forms of all of the mutants have significantly lower catalytic activities (Table 3) than wt MnSOD (*42*). Mutation of Gln146 to histidine or leucine results in the loss of more than 90% of the enzyme activity. Q146E was isolated as an apoprotein lacking SOD activity. Y34A was isolated mainly as the reduced Mn(II) form, but retaining the full activity of wt MnSOD. The reduced Mn(II) metal center in Y34A can be oxidized by the powerful oxidant, $NaIO_4$, to the Mn(III) form with loss of ∼5−10% of the SOD activity.

The Fe-substituted mutants have considerably lower activity than their Mn-containing counterparts, except for Q146H (Table 3) for which the Fe and Mn complexes have comparable activity at pH 7.8. When the pH of the SOD assay buffer was lowered from 7.8 to 6.5, the activity of Fe_2-Q146H-MnSOD more than doubled but the activity of Mn_2-Q146H-MnSOD did not change.

Active Site Spectra of MnSOD Mutants. The optical absorption spectra at pH 7 of the Mn(III) forms of Y34F and Y34A closely resemble the spectrum of wt Mn(III)SOD, having a maximum absorption peak near 480 nm with extinction coefficients of 780 and 700 M^{-1} cm^{-1}, respectively, slightly lower than the value of 850 M^{-1} cm^{-1} for the wt enzyme (*52*). Additionally, Y34A-MnSOD has a broader shoulder around 450 nm when compared with the wt and the Y34F-MnSOD mutant. The close correspondence of the spectra of wt, Y34A-, and Y34F-MnSOD at pH 7 correlates with the relatively minor effects on the structure produced by mutation of Y34 (see below). However, neither the Y34F nor the Y34A mutant exhibits the significant (33%) reduction in peak intensity at high pH (pH 10) observed for the wt protein (*42*), although all three proteins share a similar affinity ($K_d \sim 5$ mM) for azide at pH 7.

Optical absorption spectra of Q146H- and Q146L-Mn(III)-SOD are distinct from spectra observed for the wt enzyme (*52*), Y34F-MnSOD (*42*), and Y34A-MnSOD. For both of these Q146 mutants, the absorbance maximum is shifted to higher energy (from 480 to near 465 nm), and the partly resolved shoulder near 600 nm is about 30% lower in intensity than that observed for the wt enzyme. This shoulder is well-resolved in Q146L (Figure 3, upper solid line). Unlike wt (*52*), Y34F-Mn(III)SOD (*42*), and Y34A-Mn(III)SOD, the Mn(III) absorption spectra of both Q146H and Q146L are unchanged in the presence of NaN_3 (data not shown), but as observed for the wt enzyme (but not Y34A or Y34F), both spectra are sensitive to pH (Figure 3, upper dashed line). At high pH, both absorption spectra decrease in intensity by approximately one-third. The absorption maximum also shifts to higher energy (Figure 3, upper dashed line), which is characteristic of the azide adduct of the wt protein rather than the high-pH complex (*42*). The pK_a values for these conversions (pK_a = 10 for Q146L, pK_a = 9 for Q146H, Figure 3, inset) are close to the value observed for the wt enzyme (pK_a = 9.7).

At least four transitions are resolved in circular dichroism spectra of both Q146H- and Q146L-Mn(III)SOD in the

Table 4: Selected Interatomic Contacts (Å) Associated with His146 in *E. coli* Q146H-MnSOD, *Pr. shermanii* MnSOD, *M. tuberculosis* FeSOD, and *S. solfataricus* FeSOD[a]

				Q146H	*Pr. shermanii*	*M. tuberculosis*	*S. solfataricus*
Mn206	Mn	OH207	OH	2.31 (4)	2.1	2.29 (8)	2.32
His146	NE2	OH207	OH	2.78 (5)	–	–	–
	CE1	OH207	OH	–	3.11	3.19 (12)	3.10
His146	CE1	Tyr34	OH	3.6	–	–	–
	NE2	Tyr34	OH	–	3.11	3.00 (6)	2.88
His146	CD2	Trp128	NE1	3.6	–	–	–
	ND1	Trp128	NE1	–	3.00	2.95 (6)	2.94
His146	ND1	Asn73	O	3.02 (3)	–	–	–
	CD2	Asn73	O	–	long	3.75 (13)	3.32

[a] Values given are the means of the NCS-related hydrogen bond distances. For structures with more than two NCS-related chains, the standard deviations of the NCS-related values are given in brackets. Weakly active *E. coli* Q146H-MnSOD has a different orientation of its His146 ring (rotation of ~180° around χ_2) relative to the histidine rings of the active His146 SODs. Residues equivalent to *E. coli* MnSOD residues His146, Asn73, Trp128, and Tyr34 are *Pr. shermanii* FeSOD (PDB entry 1AR5) His146, Phe67, Trp126, and Tyr35; *M. tuberculosis* FeSOD (PDB entry 1IDS) His145, Phe68, Trp125, and Tyr36; and *S. solfataricus* FeSOD (PDB entry 1SSS) His155, Asn154, Trp135, and Tyr41, respectively. The covalent bond distance between the metal and its bound solvent is also given. Note that His146 of the cambialistic *Pr. shermanii* FeSOD has been rotated by 180° about χ_1 (see the Discussion).

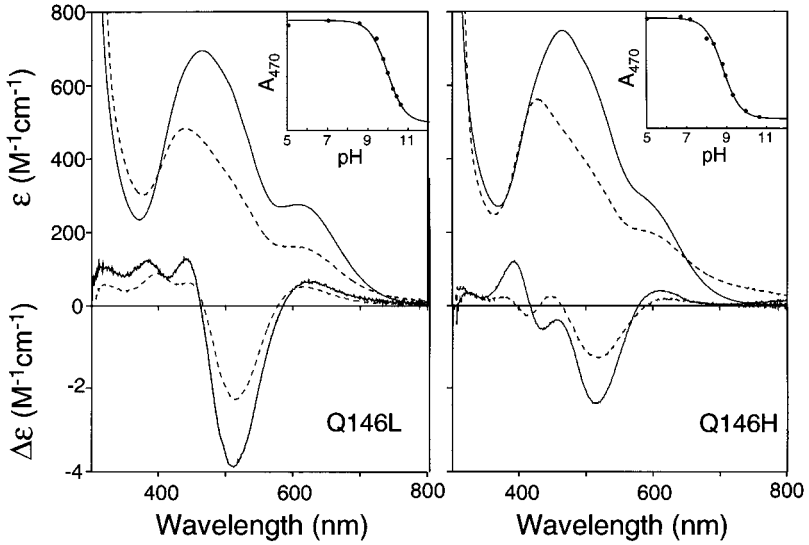

FIGURE 3: Optical spectra of Q146H- and Q146L-MnSOD. (Upper left) Optical absorption spectra of Q146L: (—) 0.45 mM active site in 50 mM potassium phosphate at pH 7.0, (- - -) 0.45 mM active site in 50 mM CAPS/KOH at pH 10.5, and (inset) pH titration of the optical spectrum, where the protein (0.2 mM active site) was prepared in the following buffer (100 mM) adjusted to an ionic strength μ of 1 with Na_2SO_4, potassium acetate (pH 5.0), potassium phosphate (pH 7.0 and 8.53), or CAPS/KOH (pH 9.37, 9.7, 9.96, 10.18, 10.37, and 10.6). (Upper right) Optical spectra of Q146H: (—) 0.44 mM active site in 50 mM potassium phosphate at pH 7.0, (- - -) 0.44 mM active site in 50 mM CAPS/KOH at pH 10.5, and (inset) pH titration of the optical spectrum, where the protein (0.2 mM active site) was prepared as described above, with potassium acetate (pH 5.0), potassium phosphate (pH 6.7, 7.18, and 8.35), Bicine/KOH (pH 8.0, 8.8, and 8.94), or CAPS/KOH (pH 9.33, 9.97, and 10.6). (Lower left) Circular dichroism spectra of Q146L: (—) 1 mM active site in 50 mM potassium phosphate at pH 7.0 and (- - -) 1 mM active site in 50 mM CAPS/KOH at pH 10.5. (Lower right) CD spectra of Q146H: (—) 1 mM active site in 50 mM potassium phosphate at pH 7.0 and (- - -) 0.72 mM active site in 50 mM CAPS/KOH at pH 10.5.

region between 300 and 800 nm (Figure 3, lower solid line). The CD spectrum of Q146L closely resembles that of wt Mn(III)SOD in both the intensity and energy of the extrema, although the strongest CD transition is shifted from 535 to 515 nm. This shift leads to relatively low intensity near 550 nm in the absorption spectrum, resulting in partial resolution of the lowest-energy ligand field feature near 600 nm. For the Q146H-MnSOD mutant, there is a dramatic reduction in the intensity of the 515 nm CD band, even though there is no significant difference in absorption spectra between those two mutant proteins. As for the optical absorption spectra, the CD spectra of both proteins are unchanged in the presence of NaN_3 and the CD intensity decreased for both spectra at high pH (Figure 3, lower dashed line).

The oxidized Mn(III) complexes of Q146H and Q146L give rise to intense paramagnetic MCD spectra at low temperatures (Figure 4), with four principal electronic transitions resolved in the region between 350 and 800 nm. For Q146L-MnSOD, MCD features occur at 390, 460, 512, and 600 nm, while for Q146H-MnSOD, the corresponding features lie at 385, 457, 520, and 575 nm. The intensity of these features ($\Delta\epsilon_{MCD,460nm} = 12.9\ M^{-1}\ cm^{-1}\ T^{-1}$ for Q146L and $\Delta\epsilon_{MCD,457nm} = 13.6\ M^{-1}\ cm^{-1}\ T^{-1}$ for Q146H) is typical of MCD arising within the high-spin Mn(III) ground state. The regions of positive and negative intensity are roughly equal over the spectra, but the pattern of intensity is different for the two complexes, with a stronger contribution from the feature near 512 nm in the Q146L mutant. The reduced Mn(II) complexes are also paramagnetic, giving rise to EPR spectra that are very similar to those observed for the wt enzyme (data not shown).

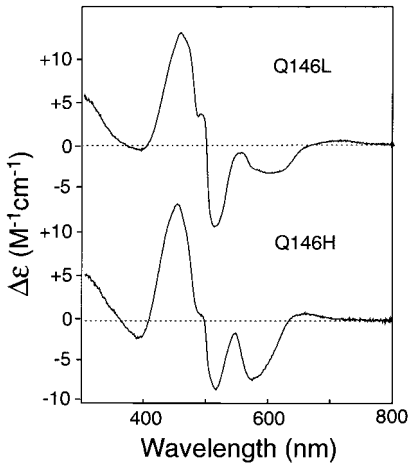

FIGURE 4: MCD spectra of Q146H- and Q146L-MnSOD. (Top) Q146L (3.5 mM active site) in 50% glycerol and 25 mM potassium phosphate buffer (pH 7.0), with MCD recorded at 4.6 K with a magnetic field of 1.0 T. (Bottom) Q146H (3.0 mM active site) in 50% glycerol and 25 mM potassium phosphate buffer (pH 7.0), with MCD recorded at 4.3 K with a magnetic field 1.0 T.

The distinct optical spectra observed for the Q146H and Q146L mutants correlate with structural data (see below), showing that mutation of Gln146 has a greater effect on protein structure than mutation of Tyr34, resulting in rearrangement of neighboring groups.

General Comments on the Structural Results. All three mutant structures have at least 89% of residues in the most favored regions of the Ramachandran plot (Table 2) (*60*). In all mutant structures (and wt), Asn145 was in a normally disallowed region ($\varphi \sim 45°$, $\psi \sim -120°$) and Gln178 (and in several chains Lys204) lay in a generously allowed region. For each structure, the pairwise rms differences among the 820 main chain atoms (N, CA, C, and O) of the four subunits range between 0.14 and 0.48 Å (Table 2). Consistent with the facts that the mutations are conservative and/or approximately isosteric, interior to the enzyme, and not directly involved in the interface forming the dimer or in dimer−dimer contacts, the quaternary structures of wt and mutant dimers are highly similar. Pairwise comparison of the two dimers of wt with the two dimers of the mutant structure leads to rms deviations for the 1620 main chain atoms that comprise each dimer in the range of 0.35−0.61 Å. Regions of greatest difference between monomers are concentrated at the N-terminus, the loop between the first and second helices, residues 134−136 (involved in dimer−dimer contacts), and the C-terminus.

Metal−ligand bond lengths in the mutant and wt structures are very similar with the differences in the bond lengths ranging from −0.05 to 0.06 Å, most differences being in the same range as the standard deviations of the values when compared over the four subunits, typically, ∼0.03 Å. Here and elsewhere, the number in parentheses following an average value for interatomic separations, bond angle, or torsion angle is the estimated standard deviation for the scatter of the values about their mean for the four subunits of the asymmetric unit; viz., 2.71 (3) Å denotes an esd of ±0.03 Å in the mean value of 2.71 Å. For the Y34F mutant, a systematic decrease in metal−ligand bond lengths averaging 0.04 Å is seen, possibly representing a higher proportion of Mn(III) in the Y34F mutant than in wt. For the Q146H and, to a lesser extent, Q146L mutants, there are significant changes in bond angles and torsion angles in the first and second coordination shells, relative to wt and Y34F-MnSOD. These changes are described in detail below.

Structural Description of Y34F. Tyr34 is absolutely conserved in all Fe- and MnSODs. The phenolic oxygen of this residue lies 5.40 (2) Å from the metal, and forms part of the hydrogen-bonding relay linking the metal with solvent in the substrate access funnel via Gln146 and the metal-bound hydroxide. Mutation of Tyr34 to phenylalanine causes only small rearrangements of the residues in and around the active site. The hydrogen bonds of Tyr34 OH with Gln146 NE2 and with a water in the substrate access funnel of the wt MnSOD are absent in the Y34F mutant. No water is observed to move into or near the site vacated by the OH of Tyr34 in the Y34F mutant. Despite the loss of these position-restraining hydrogen bonds, coupled with the change in the steric and polar character for this residue, negligible changes occur in the positioning of the phenyl ring between wt and Y34F-MnSOD structures. There is a shift of 0.4 Å for the CZ carbon of the phenyl ring (Figure 5a). Both Tyr34 and Phe34 are positioned identically in the four subunits, leading to identical positioning of Gln146. Consequently, there is also no change in the hydrogen bond between Gln146 NE2 and the metal-bound solvent [2.91 (4) Å in wt and 2.86 (11) Å in Y34F-MnSOD].

The water structure is highly conserved in Y34F-MnSOD, despite the absence of a hydrogen bond between Tyr34 OH and the water in the substrate access funnel. Of the 16 waters in the substrate access funnel of Y34F, 15 can be found in equivalent positions in the wt structure (Figure 5b). There is only one additional water unique to the Y34F structure, being found in chains B−D near the edge of the substrate access funnel. Of the 17 waters in the substrate access funnel of the wt structure, two do not have a corresponding fully occupied water present in all chains (A−D) of the Y34F structure. The water involved in the hydrogen bond with Tyr34 of wt is very well ordered, having an average *B*-factor of 18 Å^2 (compared with the average solvent *B*-factor in the structure of 32 Å^2). In Y34F, this water is seen at full occupancy only in subunit C (*B*-factor = 28 Å^2), although residual electron density indicates that this water may be present at low occupancy in subunit D. The wt structure also has another water near Tyr34, but it is located 3.5 Å from the phenolic oxygen and in a poor geometry for a hydrogen bond. This water is only seen in subunits B and D of the wt structure and not at all in Y34F.

The position of Phe34 does not leave sufficient room for a water to hydrogen bond directly with the NE2 nitrogen of Gln146, replacing the tyrosine phenolic OH. Such a water would have unfavorably close (2.7−3.0 Å) contacts with carbon atoms on Phe34 and Trp169. Accordingly, no water density is seen close to the site vacated by the phenolic OH, except that there is some weak residual density (2−3σ level in a $1|F_o| - |F_c|$ electron density map) in one subunit (D) that has not been fully accounted for.

Structural Description of Q146H. Gln146 is an important outer sphere residue, its side chain forming a second-shell hydrogen bond with the metal-coordinated solvent molecule. This hydrogen bond is conserved in all Fe- and MnSODs irrespective of whether this residue is Gln or His. In the wt structure, Gln146 makes four hydrogen bonds, involving both

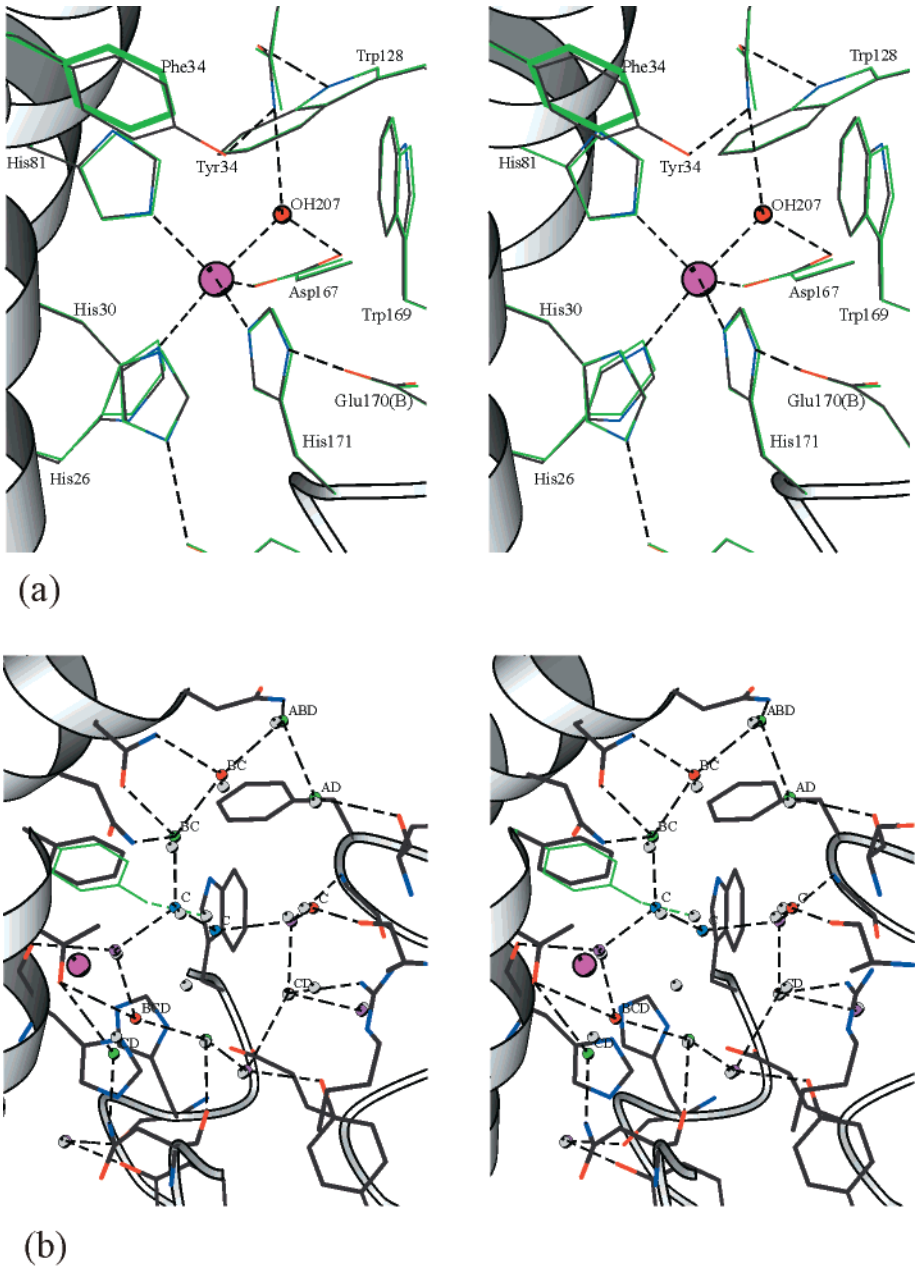

FIGURE 5: Active site changes for the Y34F mutant of MnSOD. (a) A stereodiagram showing an overlay of Y34F subunit A (green) and wt subunit A (colored by atom type) in the region of the mutation. The mutated residue Phe34 is shown in thick green lines. The largest change is in Phe34, undergoing rotation in χ_1 by 3−4°. The Mn ion is represented by the larger purple sphere and its coordinated solvent by the smaller red sphere. (b) The 16 waters in the substrate access funnel of Y34F are colored by *B*-factor: $B < 25$ Å^2, purple; $B < 26-30$ Å^2, blue; $B < 31-35$ Å^2, green; and $B > 35$ Å^2, red. The average *B* for solvent in the protein is 28 Å^2 and for the 16 waters in the substrate-access funnel is 30 Å^2. The unique waters in the substrate access funnel of the wt structure are superimposed for comparison, and drawn as gray spheres. Tyr34 of the wt structure is shown in green, along with its hydrogen bond to a water in the substrate access funnel. Labels on water molecules indicate that an ordered water molecule was not found in all four subunits at this position. The label lists the subunits in which ordered water molecules were found. No label indicates the water was present in all four subunits. The Mn ion is represented by the larger purple sphere. This figure was drawn with MOLSCRIPT (*71*).

oxygen and nitrogen atoms of the amide side chain. The NE2 nitrogen of Gln146 is the donor in hydrogen bonds with the metal-coordinated solvent [2.91 (4) Å] and the phenolic oxygen of Tyr34 [3.00 (5) Å]. The OE1 oxygen of Gln146 is an acceptor in a hydrogen bond with the NE1 nitrogen of Trp128 [3.00 (4) Å] and a weaker hydrogen bond [3.36 (3) Å] with the ND2 nitrogen of Asn80 (Figure 6a). In the mutation to histidine, three of these four hydrogen bonds are lost, with only the hydrogen bond to the metal-coordinated solvent remaining. The orientation of His146 is unequivocally determined by the 3.02 (3) Å hydrogen bond between His146 ND1 and Asn73 O. Moreover, the alternative orientation leads to very weak (∼3.6 Å) hydrogen bonds (His146 ND1···Trp128 NE1 and His146 NE2···Tyr34 OH) and to an unreasonably short distance of 2.78 (5) Å between the His146 CE1 and the coordinated solvent species OH207 O. The modeled orientation, therefore, requires that His146 ND1 be an amine (NH) moiety, being hydrogen-bonded to a carbonyl oxygen. The location of the proton in the hydrogen bond between His146 NE2 and OH207 O is, however, more complex. The OH207 O···Asp167 OD1 distance is increased by more than 0.4 Å from 2.83 (3) Å in

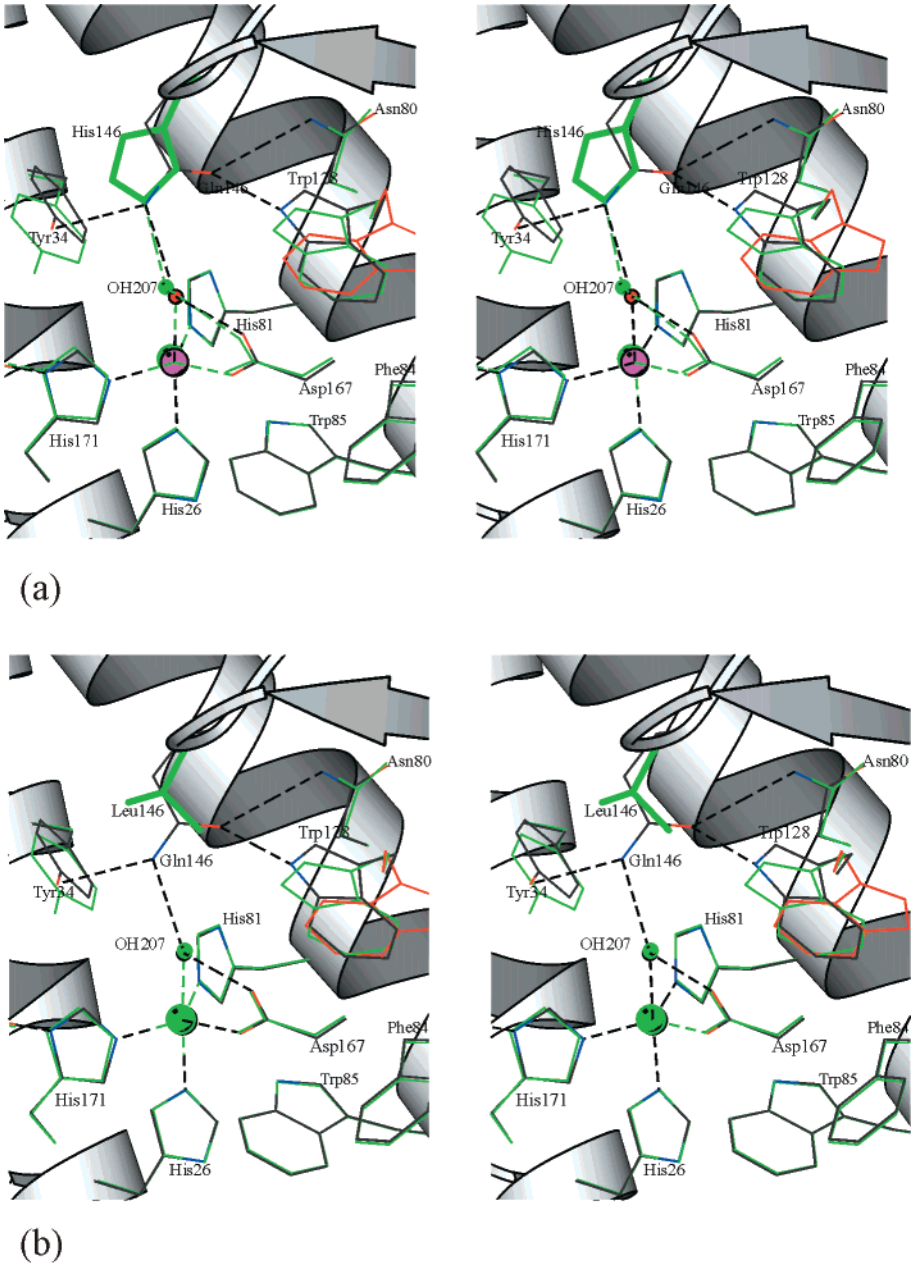

FIGURE 6: Active site changes in the Q146X-MnSOD mutants. (a) A stereodiagram showing an overlay of Q146H and the wt structure in the region of the mutation. Q146H structure in green (alternate conformation of Trp128 in red) and wt structure colored by atom type. The Mn ion of the wt structure is colored purple. See the legend of Figure 5 for labeling of water molecules. (b) A stereodiagram showing an overlay of Q146L and the wt structure in the region of the mutation. Q146L structure in green (alternative conformation of Trp128 in red) and the wt structure colored by atom type. This figure was drawn with MOLSCRIPT (*71*).

wt [2.83 (8) Å in Y34F] to 3.26 (5) Å in Q146H, a separation that is ambiguous with respect to whether a hydrogen bond still exists between the OH and the carboxyl oxygen of Asp167 in Q146H-MnSOD. This lengthening is effected by a substantial displacement of the coordinated solvent moiety by ~0.4 Å relative to the wt and Y34F structures and a small rotation of the side chain of Asp167, as is apparent in Figure 6a. These changes open up the OH207−Mn−Asp167 OD2 bond angle from 85 (1)° in wt [85 (2)° in Y34F] to 91 (1)° in Q146H-MnSOD. If a coordinated hydroxide moiety with the proton mediating a hydrogen bond between OH206 OH and Asp167 OD1 is assumed, then either atom His146 NE1 or OH207 O carries an extra proton to mediate the His146 NE1···OH207 O hydrogen bond, leading to either an imidazolium cation for His146 or an aquo species for the coordinated solvent. The latter formulation is preferred, because Q146L-MnSOD, for which no comparable hydrogen bonding with OH207 is observed (see below), and Q146H-MnSOD both exhibit similar spectral differences compared to wt MnSOD at pH 7, similar large spectral changes between pH 7 and 10.5, and a similar absence of spectroscopic evidence for azide binding.

The rotamer adopted by His146 in *E. coli* MnSOD coupled with the absence of a hydrogen bond to Tyr34 OH causes a substantial rotation of the Tyr34 side chain into the substrate access funnel, relative to wt or *E. coli* Y34F-MnSOD. The phenolic oxygen shifts by 1.5 Å and causes changes in the positions of ordered solvents within the substrate access

funnel, but this shift does not affect the positions of any other side chains (Figure 6a). The side chain of Tyr34 forms a 2.8 Å hydrogen bond with an ordered water in the substrate access funnel, the hydrogen bond being present in all four subunits. In the mutant structure, the phenolic oxygen lies only 3.7 Å from the ND1 nitrogen of His30, but the proximity of the tyrosine to the histidine does not affect the position of His30, which maintains its hydrogen bond to the phenolic oxygen of Tyr174 across the dimer interface. The movement of Tyr34 into the substrate access channel leads to a decrease of more than 0.5 Å in the Mn···Tyr34 OH separation from 5.40 (2) Å in wt to 4.86 (2) Å in Q146H.

The hydrogen bonds between the OE1 oxygen of Gln146 and residues Asn80 and Trp128 are not conserved on the mutation of Gln146 to histidine. As a consequence, the Asn80 side chain rotates 20 (4)° in χ_2, lengthening the hydrogen bond to the main chain oxygen of Gln(His)146 from 3.01 (5) to 3.37 (5) Å and allowing the ND2 nitrogen of Asn80 to act as a donor in a 3.29 (5) Å hydrogen bond to the main chain oxygen of Asp147. The hydrogen bond between Asn80 OD1 and a buried water is preserved in the Q146H mutant. The loss of the hydrogen bond between Gln146 and the side chain of Trp128 has a dramatic effect on the orientation of Trp128, which in Q146H-MnSOD adopts a discrete alternate orientation with approximately 50% occupancy. Trp128 lies in a large solvent-excluded cavity, and this alternate conformation corresponds to a flip of the indole ring. Neither conformation allows Trp128 to form hydrogen bonds with His146. The repositioning of Trp128 causes a slight rotation of Trp130 to relieve steric repulsion.

The main chain of the first half of helix A2 in the Q146H structure deviates from the wt structure. The shift at the start of the helix (residue 66) is up to 1.0 Å, but the deviation becomes negligible (0.1−0.2 Å) by residue 77. The main chain shift is accompanied by the formation of a 3.02 (3) Å hydrogen bond between Asn73 O and His146 ND1. The side chain of Phe124, which forms part of the lip of the substrate access funnel, also shifts to reoptimize its packing against the side chain of Asn73.

Structural Description of Q146L. The leucine side-chain has no hydrogen bond acceptor or donor atoms, so the four hydrogen bonds that Gln146 makes in the wt structure cannot be made when the glutamine is mutated to leucine. The leucine side chain is one methylene carbon shorter than glutamine, and has sp^3 hybridization of its CG carbon as compared with the sp^2 hybridization of the CD carbon of glutamine, affording the leucine a similar steric bulk. The leucine is, however, a hydrophobic residue, so would be expected to prefer residue packing contacts different from that of the polar glutamine. Leu146 adopts a rotamer (Figure 6b) similar to Gln146, having similar values for the χ_1 torsion angle of −68 (1)° and −68 (2)°, respectively. The χ_2 torsion angle is largely determined by side chain packing contacts of which there are nine between 3.1 and 3.8 Å. The closest approach of Leu146 to the coordinated solvent species is 3.59 (5) Å, via atom CD2. There is no evidence for water, or any other moiety, in hydrogen-bonding contact with the coordinated solvent species in three of the four subunits. In subunit C, however, a relatively poorly defined water (B = 40 Å^2) is found 2.7 Å from the coordinated solvent species and 2.5 Å from Tyr34 OH.

Relative to wt, the side chain of Tyr34 rotates into the solvent access funnel like that seen in Q146H-MnSOD. These rotations relieve steric repulsion with the CD1 carbon of Leu146, leading to comfortable van der Waals contacts between the side chains of Leu146 and Tyr34 in the range of 3.5−3.8 Å. As in Q146H-MnSOD, the ND2 nitrogen of Asn80 forms a 3.04 (8) Å hydrogen bond with the main chain oxygen of Asp147, at the expense of the hydrogen bond between Asn80 ND2 and the main chain oxygen of residue 146, and Trp128, without the hydrogen bond to residue 146, adopts an alternate conformation (Figure 6).

The separation between the coordinated solvent species and the carbonyl oxygen atom OD1 of Asp167 of 2.85 (5) Å resembles the separations observed for wt and Y34F [2.83 (3) and 2.83 (8) Å], in contrast to Q146H where this separation is 3.26 (5) Å.

DISCUSSION

The extended active site region of manganese superoxide dismutases is highly conserved in cross-species sequence correlations involving more than 80 sequences. Of the 20 residues that have at least one atom within 7.5 Å of the metal center, nine (including the four Mn or Fe ligands) are absolutely conserved. An additional six residues are very similar (Trp → Tyr or Phe, Ala → Ser, and His → Asn). From the time that the first X-ray crystallographic structures of both iron and manganese superoxide dismutase revealed their location (*22*, *27*, *30*), two of these conserved residues, Tyr34 and Gln146, have been implicated as playing an important role in the catalytic fine-tuning of these enzymes, largely based on their proximity to the metal center and their involvement in a conserved hydrogen-bonding pattern in the active site. Residues in the secondary coordination sphere are known to modulate the behavior of the metal via their interactions with directly coordinating metal ligands, fine-tuning the enzyme by defining the orientation of critical residues, modifying the redox properties of the metal center, altering substrate interactions, and affecting metal charge stabilization, all of which affect catalytic activity (*61*−*67*).

Tyr34, which is absolutely conserved in iron and manganese superoxide dismutase sequences, is positioned with its phenolic oxygen only 5.4 Å from the metal center, forming a hydrogen bond with the amide nitrogen of Gln146 (or its structurally equivalent residue). The amide nitrogen of Gln146 lies 4.7 Å from the metal and forms another hydrogen bond to a solvent molecule that is covalently bonded to the metal. This solvent molecule, H_2O or HO^- depending on the oxidation state of the metal ion, completes a hydrogen-bonding relay extending from the solvent surrounding the enzyme to the metal ion via Tyr34, Gln146, and the metal-bound solvent. Protons are involved in the mechanism of superoxide dismutation, and the hydrogen-bonding relay may function to deliver protons to oxyanion intermediates during turnover (*42*). In both Mn- and FeSODs, this functional group can be provided by either a glutamine or a histidine, although this residue is not always part of the same secondary structure element. In the structures determined to date and for more than 20 FeSOD and 65 MnSOD sequences, the following pattern is observed, with alignments yet to be confirmed by three-dimensional structure determinations in brackets. In MnSODs, the residue occupying the position equivalent to

Gln146 is always either a glutamine or a histidine, and the position equivalent to Gly77 is always a glycine. In FeSODs, the position equivalent to Gln146 is either a histidine (or glutamine) or an alanine (or, very rarely, glycine), in which case the residue at the position equivalent to Gly77 is a glycine or glutamine, respectively. However, no Fe- or MnSOD has so far been observed to have a histidine at residue 77, nor has a glutamine been observed at residue 77 in any MnSOD.

The effect that these two active site residues has on the function of the enzyme has been tested by their selective replacement. This work presents the X-ray crystallographic structures of three active site mutants, Y34F, Q146H, and Q146L. While this work was in progress, structural and functional studies were published by other groups on the Y34F, Q143N, and Q143A mutants of human mitochondrial MnSOD (*45*, *46*, *49*) and on the H145Q and H145E mutants of the FeSOD from *M. tuberculosis* (*50*). These studies complement the work reported there and permit a deeper analysis of the role of these residues in enzyme function.

Y34X Mutants. The substitution of phenylalanine for tyrosine in Y34F-MnSOD eliminates structurally important hydrogen bonds to Gln146 and solvent in the substrate access funnel. Nonetheless, solvent structure in the substrate access funnel is very similar except that the water that forms a hydrogen bond with Tyr34 OH in the wt MnSOD is less ordered in the Y34F mutant. No additional solvent diffuses into the active site to maintain the hydrogen bond relay linking the Tyr34 to the metal ion via Gln146, and the metal-bound solvent molecule. This proposed hydrogen bond relay from the substrate access funnel to the metal is thus completely disrupted by the mutation. However, this disruption is accompanied by an only ~20% loss of activity at pH 7.8 and 9.0, implying that Gln146, along with other polar groups in the active site, is sufficient to provide a proton-hopping pathway into the solvent pocket during turnover. The activity of the Y34A mutant is insignificantly different at pH 7.8 from that of wt MnSOD from *E. coli*. At pH 7, the UV−visible spectra of wt, Y34F (*42*), and Y34A are very similar. However, at pH 10.5, the extinction coefficient at 480 nm has decreased by approximately 30% in wt but by less than 10% in Y34F and Y34A. Similar diminutions are observed for the wt and Y34F mutants of the MnSOD from human mitochondria (*45*). It has proved tempting to assign this large spectral change for the wild type, which has a pK_a of ~9.7, to deprotonation of the hydroxyl group of Tyr34, and the smaller spectral changes of the mutants, which have a similar pK_a of ~10, to coordination of hydroxide at the sixth site (*45*). However, as argued earlier (*42*), binding of hydroxide to Y34F- and Y34A-MnSOD has a pK of >11, by analogy with the pH-dependent spectral changes of Fe_2-MnSOD and Fe_2-Y34F-MnSOD. The smaller spectral change seen at pH ~7 in Y34A- and Y34F-MnSOD may be attributed to a protonation event at, most likely, His30.

Azide affinities for the Y34F and Y34A mutant complexes are 1.5−4 times higher than for the corresponding complexes of wt MnSOD (*42*). Azide provides a useful probe of exogenous ligand interactions in the active site that may mimic substrate (superoxide) or product (peroxide) interactions. Substrate binding is affected by both steric and electrostatic factors, including substrate−protein interactions and charge stabilization of the metal center. Tighter binding of azide in Y34F and Y34A mutants could be due to an overall more positive charge on the metal center, or relaxed steric constraints in the substrate funnel resulting from deletion of the tyrosine OH. Although azide has been shown to bind to both wt and Y34F *E. coli* MnSOD in solution, it has not been possible to detect the azide in these species by X-ray crystallography

Hydrogen-Bonding Patterns of Wild-Type and Mutant SODs with Histidine at Position 146. Mutagenesis of residues that interact with the coordinated solvent species has a greater effect on catalysis, the activity of Q146H-MnSOD being only 10% of that of the wt enzyme. Further, the iron-substituted mutant has activity comparable to that of the manganese form (Table 3), typical of cambialistic superoxide dismutases. The SOD activity of Fe-substituted Q146H-MnSOD increased at lower pH, while activity of the manganese form is relatively constant. Thus, the *E. coli* Q146H-MnSOD mutant exhibits behavior similar to that found for the subfamily of metal-nonspecific (cambialistic) SODs from *Streptococcus mutans* (*15*), *Mycobacterium smegmatis* (*19*), *Aeropyrum pernix* (*20*), and *Pyrobaculum aerophilum* (*68*). The active site Mn(III) absorption and CD spectra of Q146H-MnSOD also resemble spectra observed for the cambialistic SOD from *P. aerophilum* (*68*), which has a histidine rather than a glutamine in the solvent pocket. Thus, the anomalously low CD intensity and peak extrema of the Q146H mutant may correlate with its cambialistic character, implying that the spectroscopic and catalytic features have a common origin in the electronic perturbations in this site.

In the Q146H mutant, the histidine side chain of residue 146 adopts a conformation sterically similar to that of the wt glutamine for which it substitutes (Figure 6a). Because of the different types and positions of hydrogen-bonding groups on the histidine, the hydrogen-bonding network of the wild-type enzyme is disrupted, leading to movement of Tyr34 and disorder of Trp128. Both hydrogen bonds formed between Gln146 OE1 and the residues Asn80 and Trp128 in the wt MnSOD are absent in the Q146H mutation. In the wt, Asn80 and Trp128 orient the glutamine, and also possibly modulate its character. These roles can be further examined in future mutation studies. The loss of the hydrogen bond with Trp128 causes conformational disorder of this tryptophan residue, which adopts two positions in equal amounts, the wild-type orientation and another in which the Trp128 side chain rotates ~180° around χ_1. The NE1 nitrogen of Trp128 in the new orientation seen in the Q146H mutant is not involved in any hydrogen bonds.

If the histidine is involved in modulating the character of the metal ion via the metal-bound solvent, then the orientation of His146, and its hydrogen bonds, becomes important. The orientation of His146 in the weakly active and somewhat cambialistic *E. coli* Q146H-MnSOD mutant can be assigned unambiguously (see the Results). This orientation, which places atom His146 NE2 in hydrogen-bonding contact with the coordinated solvent moiety, is *not* the orientation observed in three FeSODs. In *S. solfataricus* FeSOD (PDB entry 1SSS) (*37*), *S. acidocaldarius* (PDB entry 1B06) (*38*), and *M. tuberculosis* FeSOD (PDB entry 1IDS) (*33*) structures, the histidine is oriented to place atom CE1 close to the coordinated hydroxide (Figure 7B). This leads to sensible hydrogen-bonding distances for the histidine imine and amine

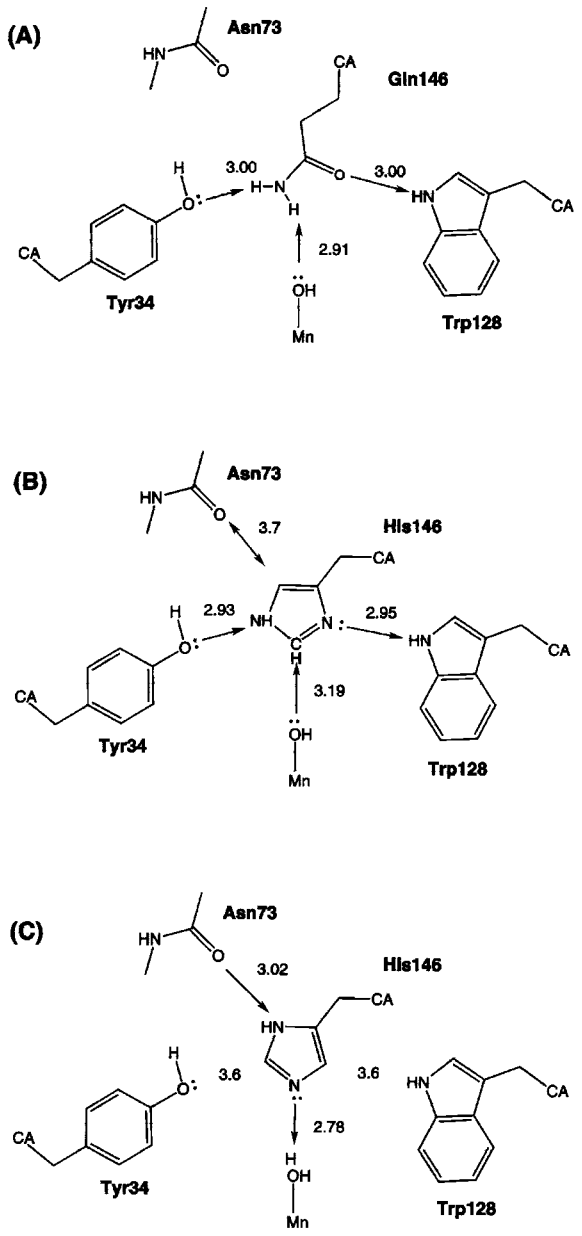

FIGURE 7: Schematic of hydrogen bonding around residue 146 (His or Gln). (A) Active wt *E. coli* MnSOD containing Gln146. (B) Active naturally occurring His146 FeSODs (*M. tuberculosis*, *S. sulfataricus*, and corrected *Pr. shermanii*). Hydrogen bond lengths are for the FeSOD from *M. tuberculosis* (PDB entry 1IDS; average of four subunits). (C) Weakly active Q146H *E. coli* MnSOD. Both active forms (A and B) share common features, a hydrogen bond between a nonacidic (aprotic) proton donor on residue 146 and the metal OH^- ligand, a hydrogen bond between residue 146 (donor) and Tyr34 OH (acceptor), and a strong hydrogen bond between residue 146 (acceptor) and the adjacent tryptophan (donor). The inactive form (C) lacks both the hydrogen bond with the tyrosine and the hydrogen bond with the tryptophan, and has a strong hydrogen bond involving a mildly acidic proton shown here attached to a metal OH^- ligand. Alternatively, this proton may be attached to the imine nitrogen of the imidazole ring.

moieties to the adjacent Trp128 and Tyr34 residues. However, for the *Pr. shermanii* structures [PDB entries 1AR5, 1AR4, 1BS3, 1BSM, and 1BT8) (*35*, *44*, *69*)], the models that have been adopted place the His146 NE1 atom within hydrogen-bonding distance of the coordinated hydroxide. In all these structures, this then leaves an unnaturally close, non-hydrogen-bonding contact of 2.95−3.05 Å between atoms His146 CD2 and Trp128 NE2 (Figure 7C). If the histidine is modeled in the alternate conformation, two strong hydrogen bonds (His146 NE2···Tyr34 O and Trp128 NE2··· His146 ND1) and a weaker His146 CE1···OH207 OH^- interaction provide a seemingly more favorable geometry of the histidine (analogous to Figure 7B). We conclude that the conformation of this histidine is systematically wrong in these *Pr. shermanii* structures. Moreover, for the parent *Pr. shermanii* structure (PDB entry 1AR5), notwithstanding the authors' comment (*35*) that the orientation of the histidine could not be determined unambiguously, not only are the *B* values archived in the PDB for this residue very much lower than average (8−13 $Å^2$) but also their pattern is utterly consistent with nitrogen and carbon atoms being interchanged. Rotation of the imidazole by 180° about the CB−CG bond leads to the acceptable hydrogen bonding observed in the *M. tuberculosis*, *S. solfataricus*, and *S. acidocaldarius* FeSOD structures (*33*, *37*, *38*).

Role of Gln (or His) at Position 146. Comparison of the structures of wt and various site-directed mutants of iron and manganese superoxide dismutases reveals an interesting result: in all catalytically active forms of the enzyme, the hydrogen-bonding potential of the residue at position 146 is fully saturated. In all native or wt structures, the hydroxide moiety interacts with either the weakly polarized but aprotic (nonacidic) CE1-H moiety of His146 or the more strongly polarized but still aprotic NH2 moiety of Gln146 (or Gln77). The imine moiety (unprotonated nitrogen) of His146 hydrogen bonds to the H-NE1 tryptophan moiety equivalent to Trp128 of *E. coli* MnSOD; the amine moiety (protonated nitrogen) hydrogen bonds to the tyrosine equivalent to Tyr34 of *E. coli* MnSOD. Moreover, this orientation of the histidine not only strongly disfavors its protonation, because of the His ND1···H-NE1 Trp hydrogen bond, but also controls the orientation of the phenolic hydrogen on Tyr34. The glutamine NH_2 and C═O groups of Mn- and FeSODs with Gln at position 146 (or 77) perform the same function in orienting the Tyr OH group.

In the nearly inactive Q143N mutant of human MnSOD (Q146N in *E. coli* MnSOD), a (protic) water molecule (possibly H_3O^+) hydrogen bonds not only to the amide side chain but also to the tyrosine equivalent to Tyr34 of *E. coli* MnSOD and to the coordinated solvent molecule (*46*). In this mutant, the latter species is probably water, as the pH of crystallization was 4.6, and the mutant resting state is Mn(II). In the weakly active, metal-nonspecific Q146H mutant of *E. coli* MnSOD described here, the His146 is unequivocally oriented to form a hydrogen bond, probably through its imine function, only with the coordinated solvent. The H145Q-FeSOD mutant of *M. tuberculosis* has the glutamine amide oriented in a manner similar to that of Gln146 of *E. coli* (and other SODs that have a structurally equivalent Gln), as best as can be determined at 4 Å resolution with NCS constraints applied to the two crystallographically independent molecules (*50*). The H145E mutant preferentially binds manganese, and at 2.5 Å resolution, a clearer definition of residues results. The authors favor a coordinated hydroxide hydrogen-bonded to an anionic Glu145 side chain, which in turn hydrogen bonds to Tyr36 (equivalent to Tyr34 of *E. coli* MnSOD) (*50*). However, this alters the inferred locations of the hydroxide and Tyr OH hydrogen atoms. Even at pH 7.0−7.6, the pH of crystallizations,

protonation of Glu145 or of the coordinated solvent species seems more likely, especially as both this and the H145Q mutants are described as active, and the hydrogen bond between the coordinated solvent species and the carboxyl oxygen of the aspartate ligand is, presumably, preserved.

Thus, in native or wt Mn- and FeSODs, the major role of the histidine or glutamine side chains structurally equivalent to Gln146 of *E. coli* MnSOD appears to be the orientation and polarization of the Mn−OH bond of the coordinated solvent. The bulk of the side chain also buttresses the Tyr34 group, preventing closer approach of Tyr34 to the metal center. These effects appear directed to facilitating step 1b, the oxidation of the metal, and the reduction and protonation of superoxide to give hydrogen peroxide. In the reduced complex, the coordinated solvent is water, with the second proton likely occupying the open trigonal site defined by interactions with Gln146 and Asp167. Gln146 (a hydrogen bond donor) and Asp167 (a hydrogen bond acceptor) control the reactivity of the coordinated solvent in the $M(OH_x)$ unit, with the remaining lone pair of electrons on the oxygen atom of the coordinated solvent open for exogenous protonation during turnover. Protonation at this position would be consistent with previous density functional theory calculations on the active site (*70*). Proton transfers in and out of the buried solvent pocket may be facilitated by the side chains that form the base of the substrate funnel. The combined effects of Tyr34 and Gln146 (or equivalent Tyr and His) are to facilitate departure and protonation of the peroxide. A secondary role for the polar residue at position 146 appears to be in tuning activity of the metal by placing an electropositive but nonprotic moiety (histidine C-H or glutamine amide NH_2) approximately 4.7 Å from the metal. The Q143N mutant of human MnSOD and the Q146L mutant of *E. coli* MnSOD are both more easily reduced than wt or other mutants. In the case of the human MnSOD, the pH of crystal growth (pH 4.6) makes it likely that the water molecule that fills the space vacated by the Q146N mutation is protonated. In the case of weakly active Q146L for the MnSOD from *E. coli*, the coordinated OH (or more likely H_2O) hydrogen bonds only to the carboxyl of the ligand Asp167.

The Q146L-MnSOD mutation is nearly isosteric with wt MnSOD, despite being one methylene carbon shorter. Not being completely isosteric makes it more difficult to distinguish between changes due to the loss of all hydrogen-bonding groups, and those due to steric repulsion from the different atomic arrangement. Rearrangements occur for Tyr34, Asn80, and Trp128, largely due to the loss of hydrogen bonds between these residues and Leu146. Tyr34 moves toward the substrate access funnel due to repulsion from the CD1 carbon of leucine, constricting the volume of the sixth coordination site at the Mn. In both the Q146H and Q146L mutants, the rotation of Tyr34 can be determined to be entirely due to steric repulsion from residue 146, rather than loss of a hydrogen bond to the same residue. Movement of Tyr34 due to loss of the hydrogen bond can be discounted as Phe34 in the Y34F mutant undergoes very little rotation, and in fact rotates toward residue Gln146.

The bond length between Mn and the coordinated solvent species (207OH) is largely unaffected by both the Q146H and Q146L mutations, having bond distances [2.31 (4) and 2.31 (2) Å, respectively] comparable to that of wt [2.27 (3) Å]. This is despite the fact that mutation of residue 146 modifies the ligand field strength of the metal as seen by changes in the optical spectra. The rotation of Tyr34 into the solvent access funnel constricts the volume of the sixth coordination site at the metal center. In all native or wild-type structures with unmodified Tyr34 (*21*−*29*, *33*−*36*, *38*), this distance falls between 5.2 and 5.5 Å [5.40 (2) Å in wt MnSOD from *E. coli*] (*26*, *59*). However, in the *E. coli* Q146H and Q146L mutants, this distance decreases to 4.86 (2) and 4.92 (4) Å, respectively. This reduction in size of the binding cavity for the exogenous sixth ligand may be a significant factor contributing to the diminished activity of these mutants, and to the inability of these mutants to bind azide.

CONCLUSIONS

The Y34F and Y34A mutations of the MnSOD from *E. coli* have little effect on superoxide dismutase activity, azide binding, or, in the case of Y34F, the structure, but shift the pK_a for the binding of hydroxide to the sixth coordination site of Mn to >10. The Q146L mutant disrupts the hydrogen-bonding chain ($MnOH_x$···NE2 Gln146···OH Tyr34···solvent), leading to diminished activity, loss of azide binding, and significantly different optical spectra compared to those of wt, Y34F, and Y34A, although hydroxide binding is still observed with a pK_a of <10. Substantial rearrangements of active site residues occur, in particular of Tyr34, which moves into the substrate access funnel and closer to the metal ion. Similar changes occur for the Q146H mutant, but this mutant is weakly active as its Fe derivative, although the interaction of His146 to the coordinated solvent is through NE2, rather than CE1, as occurs in those Fe- and MnSODs for which His is the natural residue. Gln (or His) plays a critical role in controlling the position of Tyr34 and the orientation and polarization of the $MnOH_x$ moiety.

REFERENCES

1. McCord, J. M., and Fridovich, I. (1988) *Free Radical Biol. Med. 5*, 363−369.
2. Fridovich, I. (1995) *Annu. Rev. Biochem. 64*, 97−112.
3. Fridovich, I. (1997) *J. Biol. Chem. 272*, 18515−18517.
4. McCord, J. M., and Fridovich, I. (1969) *J. Biol. Chem. 244*, 6049−6055.
5. Yost, F. J., Jr., and Fridovich, I. (1976) *J. Biol. Chem. 248*, 4905−4908.
6. Keele, B. B., Jr., McCord, J. M., and Fridovich, I. (1970) *J. Biol. Chem. 245*, 6176−6181.
7. Young, H.-D., Kim, E.-J., Roe, J.-H., Hah, Y. C., and Kang, S.-O. (1996) *Biochem. J. 318*, 889−896.
8. McCord, J. M. (1976) *Adv. Exp. Med. Biol. 74*, 540−550.
9. Parker, M. W., Blake, C. C. F., Barra, D., Bossa, F., Schinina, M. E., Bannister, W. H., and Bannister, J. V. (1987) *Protein Eng. 1*, 393−397.
10. Parker, M. W., and Blake, C. C. F. (1988) *FEBS Lett. 229*, 377−382.
11. Jackson, S. M. J., and Cooper, J. B. (1998) *BioMetals 11*, 159−173.
12. Edwards, R. A., Whittaker, M. M., Whittaker, J. W., Jameson, G. B., and Baker, E. N. (1998) *J. Am. Chem. Soc. 120*, 9684−9685.
13. Meier, B., Barra, D., Bossa, F., Calabrese, L., and Rotilio, G. (1982) *J. Biol. Chem. 257*, 13977−13980.
14. Gregory, E. M., and Dapper, C. H. (1982) *Arch. Biochem. Biophys. 220*, 293−300.

15. Martin, M. E., Byers, B. R., Olson, M. O., Salin, M. L., Arceneaux, J. E., and Tolbert, C. (1986) *J. Biol. Chem. 261*, 9361−9367.
16. Pennington, C. D., and Gregory, E. M. (1986) *J. Bacteriol. 166*, 528−532.
17. Amano, A., Shizukuishi, S., Tamagawa, H., Iwakura, K., Tsunasawa, S., and Tsunemitsu, A. (1990) *J. Bacteriol. 172*, 1457−1463.
18. Matsumoto, T., Terauchi, K., Isobe, T., Matsuoka, K., and Yamakura, F. (1991) *Biochemistry 30*, 3210−3216.
19. Yamakura, F., Kobayashi, K., Tagawa, S., Morita, A., Imai, T., Ohmori, D., and Matsumoto, T. (1995) *Biochem. Mol. Biol. Int. 36*, 233−240.
20. Yamano, S., Sako, Y., Nomura, N., and Maruyama, T. (1999) *J. Biochem. 126*, 218−225.
21. Ludwig, M. L., Metzger, A. L., Pattridge, K. A., and Stallings, W. C. (1991) *J. Mol. Biol. 219*, 335−358.
22. Stallings, W. C., Pattridge, K. A., Strong, R. K., and Ludwig, M. L. (1985) *J. Biol. Chem. 260*, 16424−16432.
23. Parker, M. W., and Blake, C. C. F. (1988) *J. Mol. Biol. 199*, 649−661.
24. Wagner, U. G., Pattridge, K. A., Ludwig, M. L., Stallings, W. C., Werber, M. M., Oefner, F. F., and Sussman, J. L. (1993) *Protein Sci. 2*, 814−825.
25. Borgstahl, G. E. O., Parge, H. E., Hickey, M. J., Beyer, W. F., Jr., Hallewell, R. A., and Tainer, J. A. (1992) *Cell 71*, 107−118.
26. Edwards, R. A., Baker, H. M., Jameson, G. B., Whittaker, M. M., Whittaker, J. W., and Baker, E. N. (1998) *J. Biol. Inorg. Chem. 3*, 161−171.
27. Stallings, W. C., Powers, T. B., Pattridge, K. A., Fee, J. A., and Ludwig, M. L. (1983) *Proc. Natl. Acad. Sci. U.S.A. 80*, 3884−3888.
28. Carlioz, A., Ludwig, M. L., Stallings, W. C., Fee, J. A., Steinman, H. M., and Touati, D. (1988) *J. Biol. Chem. 263*, 1555−1562.
29. Lah, M. S., Dixon, M. M., Pattridge, K. A., Stallings, W. C., Fee, J. A., and Ludwig, M. L. (1995) *Biochemistry 34*, 1646−1660.
30. Ringe, D., Petsko, G. A., Yamakura, F., Suzuki, K., and Ohmori, D. (1983) *Proc. Natl. Acad. Sci. U.S.A. 80*, 3879−3883.
31. Stoddard, B. L., Howell, P. L., Ringe, D., and Petsko, G. A. (1990) *Biochemistry 29*, 8885−8893.
32. Stoddard, B. L., Ringe, D., and Petsko, G. A. (1990) *Protein Eng. 4*, 113−119.
33. Cooper, J. B., McIntyre, K., Badasso, M. O., Wood, S. P., Zhang, Y., Garbe, T. R., and Young, D. (1995) *J. Mol. Biol. 246*, 531−544.
34. Lim, J.-H., Yu, Y. G., Han, Y. S., Cho, S., Ahn, B.-Y., Kim, S.-H., and Cho, Y. (1997) *J. Mol. Biol. 270*, 259−274.
35. Schmidt, M., Meier, B., and Parak, F. (1996) *J. Biol. Inorg. Chem. 1*, 532−541.
36. Sugio, S., Hiraoka, B. Y., and Yamakura, F. (2000) *J. Biol. Chem. 267*, 3487−3495.
37. Ursby, T., Adinolfi, B. S., Al-Karadaghi, S., De Vendittis, E., and Bocchini, V. (1999) *J. Mol. Biol. 286*, 189−205.
38. Knapp, S., Kardinahl, S., Hellgren, N., Tibbelin, G., Schäfer, G., and Ladenstein, R. (1999) *J. Mol. Biol. 285*, 689−702.
39. Steinman, H. M. (1978) *J. Biol. Chem. 253*, 8708−8720.
40. Hunter, T., Ikebukuro, K., Bannister, W. H., Bannister, J. V., and Hunter, G. J. (1997) *Biochemistry 36*, 4925−4933.
41. Sorkin, D. L., Duong, D. K., and Miller, A. F. (1997) *Biochemistry 36*, 8202−8208.
42. Whittaker, M. M., and Whittaker, J. W. (1997) *Biochemistry 36*, 8923−8931.
43. Whittaker, M. M., and Whittaker, J. W. (1998) *J. Biol. Chem. 273*, 22188−22193.
44. Gabbianelli, R., Battistoni, A., Polticelli, F., Meier, B., Schmidt, M., Rotilio, G., and Desideri, A. (1997) *Protein Eng. 10*, 1067−1070.
45. Guan, Y., Hickey, M. J., Borgstahl, G. E. O., Hallewell, R. A., Lepock, J. R., O'Connor, D., Hsieh, Y., Nick, H. S., Silverman, D. N., and Tainer, J. A. (1998) *Biochemistry 37*, 4722−4730.
46. Hsieh, Y., Guan, Y., Tu, C., Bratt, P. J., Angerhofer, A., Lepock, J. R., Hickey, M. J., Tainer, J. A., Nick, H. S., and Silverman, D. N. (1998) *Biochemistry 37*, 4731−4739.
47. Cabelli, D. E., Guan, Y., Leveque, V., Hearn, A. S., Tainer, J. A., Nick, H. S., and Silverman, D. N. (1999) *Biochemistry 38*, 11686−11692.
48. Ramilo, C. A., Leveque, V., Guan, Y., Lepock, J. R., Tainer, J. A., Nick, H. S., and Silverman, D. N. (1999) *J. Biol. Chem. 274*, 27711−27716.
49. Leveque, V. J., Stroupe, M. E., Lepock, J. R., Cabelli, D. E., Tainer, J. A., Nick, H. S., and Silverman, D. N. (2000) *Biochemistry 39*, 7131−7137.
50. Bunting, K., Cooper, J. B., Badasso, M. O., Tickle, I. J., Newton, M., Wood, S. P., Zhang, Y., and Young, D. (1998) *Eur. J. Biochem. 251*, 795−803.
51. Hiraoka, B. Y., Yamakura, F., Sugio, S., and Nakayama, K. (2000) *Biochem. J. 345*, 345−350.
52. Whittaker, M. M., and Whittaker, J. W. (1991) *J. Am. Chem. Soc. 113*, 5528−5540.
53. Touati, D. (1983) *J. Bacteriol. 155*, 1078−1087.
54. Carlioz, A., and Touati, D. (1986) *EMBO J. 5*, 623−630.
55. Beyer, W. F., Jr., Reynolds, J. A., and Fridovich, I. (1989) *Biochemistry 28*, 4403−4409.
56. Otwinowski, Z., and Minor, W. (1997) *Methods Enzymol. 276*, 307−326.
57. Brunger, A. T., Adams, P., Clore, G. M., DeLano, W. L., Gros, P., Grosse-Kunstleve, R. W., Jiang, J.-S., Kuszewski, J., Nilges, M., Pannu, N. S., Read, R. J., Rice, L. M., Simonson, T., and Warren, G. L. (1998) *Acta Crystallogr. D54*, 905−921.
58. Navazza, J. (1994) *Acta Crystallogr. A50*, 157−163.
59. Edwards, R. A. (2000) Ph.D. Dissertation, Massey University, Palmerston North, New Zealand.
60. Laskowski, R., MacArthur, M., Moss, D., and Thornton, J. (1993) *J. Appl. Crystallogr. 26*, 283−291.
61. Kiefer, L. L., Paterno, S. A., and Fierke, C. A. (1995) *J. Am. Chem. Soc. 117*, 6831−6837.
62. Goodin, D. B., and McRee, D. E. (1993) *Biochemistry 32*, 3313−3324.
63. Tainer, J. A., Getzoff, E. D., Beem, K. M., Richardson, J. S., and Richardson, D. C. (1982) *J. Mol. Biol. 160*, 181−217.
64. Banci, L., Bertini, I., Cabelli, D. E., Hallewell, R. A., Tung, J. W., and Viezzoli, M. S. (1991) *Eur. J. Biochem. 196*, 123−128.
65. Wang, J. M., Mauro, M., Edwards, S. L., Oatley, S. J., Fishel, L. A., Ashford, V. A., Xuong, N. H., and Kraut, J. (1990) *Biochemistry 29*, 7160−7173.
66. Vitello, L. B., Erman, J. E., Miller, M. A., Mauro, J. M., and Kraut, J. (1992) *Biochemistry 31*, 11524−11535.
67. Lesburg, C. A., and Christianson, D. W. (1995) *J. Am. Chem. Soc. 117*, 6838−6844.
68. Whittaker, M. M., and Whittaker, J. W. (2000) *J. Biol. Inorg. Chem. 5*, 402−408.
69. Schmidt, M (1999) *Eur. J. Biochem. 262*, 111−126.
70. Whittaker, M. M., Ekberg, C. A., Edwards, R. A., Baker, E. N., Jameson, G. B., and Whittaker, J. W. (1998) *J. Phys. Chem. B 102*, 4668−4677.
71. Kraulis, P. J. (1991) *J. Appl. Crystallogr. 24*, 946−950.

BI0018943